

Contents lists available at ScienceDirect

Petroleum Science

journal homepage: www.keaipublishing.com/en/journals/petroleum-science



Original Paper

Comparative analysis of rock breakage characteristics and failure mode on conventional and conical PDC cutter cutting carbonate



Xin-Kang Fu ^a, Chao Xiong ^{a, b, c, *}, Huai-Zhong Shi ^a, Wen-Hao He ^{a, d}, Lu-Hai Wang ^a, Zhong-Wei Huang ^{a, **}

- ^a National Key Laboratory of Petroleum Resources and Engineering, China University of Petroleum-Beijing, Beijing, 102249, China
- b College of Mechanical and Storage and Transportation Engineering, China University of Petroleum-Beijing, Beijing, 102249, China
- ^c Center of Advanced Oil and Gas Equipment, China University of Petroleum-Beijing, Beijing, 102249, China
- d Beijing Key Laboratory of Optical Detection Technology for Oil and Gas, China University of Petroleum-Beijing, Beijing, 102249, China

ARTICLE INFO

Article history: Received 6 June 2024 Received in revised form 16 December 2024 Accepted 17 December 2024 Available online 18 December 2024

Edited by Jia-Jia Fei

Keywords: Conical cutter Rock breakage process Brittle fracture index Failure mode Carbonate rock

ABSTRACT

The oil and gas stored in deep and ultra-deep carbonate reservoirs is the focus of future exploration and development. Conical PDC (Polycrystalline Diamond Compact) cutter, which is a new kind of PDC cutter, can significantly improve the rate of penetration (ROP) and extend PDC bit life in hard and abrasive formations. However, the breakage characteristics and failure mode of the conical PDC cutter cutting carbonate rock is still masked. In this paper, a series of single-cutter cutting tests were carried out with the conical and conventional PDC cutters. The cutting force, rock-breaking process, surface morphology of cutting grooves and cuttings characteristic were analyzed. Based on the derived formula of the brittle fracture index, the failure model of carbonate rock was quantitatively analyzed under the action of conical and conventional cutter. The results show that the average cutting force of the conical cutter is less than that of the conventional cutter, which means greater stability of the cutting process using the conical cutter. Carbonate rock with calcite as the main component tends to generate blocky rock debris by conical cutter. The height of the cuttings generated by the conical cutter is 0.5 mm higher than that generated by the conventional cutter. The conical cutter exhibits enhanced penetration capabilities within carbonate rock. The accumulation of rock debris in front of the conventional cutter is obvious. Whereas, the conical cutter facilitates the cuttings transport, thereby alleviating drilling stickiness slip. At different cutting depths, the conical cutter consistently causes asymmetric jagged brittle tensile fracture zones on both sides of the cutting groove. Calculations based on the brittle fracture index demonstrate that the brittle fracture index of the conical cutter generally doubles that of the conventional cutter. For carbonate rock, the conical cutter displays superior utilization of brittle fracture abilities. The research findings of this work offer insights into the breakage process and failure mode of carbonate rock by the

© 2024 The Authors. Publishing services by Elsevier B.V. on behalf of KeAi Communications Co. Ltd. This is an open access article under the CC BY-NC-ND license (http://creativecommons.org/licenses/by-nc-nd/4.0/).

1. Introduction

Deep and ultra-deep carbonate reservoirs hold a considerably important position in oil and gas exploration and exploitation (Zhao et al., 2014). More than 70% of oil and gas resources are stored in the carbonate formations. Nearly 50% of proven recoverable oil

E-mail addresses: xiongc@cup.edu.cn (C. Xiong), huangzw@cup.edu.cn (Z.-W. Huang).

and gas resources are stored in deep and ultra-deep carbonate formations worldwide (Al-Shargabi et al., 2023), which is a key field for future exploration and development.

In China, marine carbonates are widely distributed and rich in oil and gas resources (Jin et al., 2018). However, these carbonate formations in China are concentrated at depths ranging from 5000 to 7000 m (Ma et al., 2017). These formations consist of challenging rocks that are hard, and poorly drillable, resulting in a low rate of penetration (ROP) and prolonged operating cycles (Zeng et al., 2023). Consequently, there is an urgent need to develop the high efficiency drill bit for carbonate rock drilling well.

^{*} Corresponding author.

^{**} Corresponding author.

PDC bits are the most widely used in oil fields around the world due to their high drilling efficiency (Rostamsowlat et al., 2022). More than 75% of drill bits footage for oil and gas well are completed with PDC bits in the world (Liu et al., 2024). Conventional cutter has a series of problems, such as serious abrasion, chipping and thermal damage, for drilling hard rock (Jamali et al., 2019). In 2022, some scholars designed a novel conical cutter to mitigate vibrations that can have an impact on drilling life and operation. The newly designed bit extends the durability limits of PDC bits in drilling hard, wear-resistant sandstone formations (Sun et al., 2014). As shown in Fig. 1, the conical and conventional PDC cutters are mixed arranged to form the hybrid PDC drill bits. The application of oil field proves that this kind hybrid PDC bit can significantly improve the footage and ROP in hard and interbed formation (Radhakrishnan et al., 2016).

Since the invention of conical cutter, many researchers have conducted a lot of research work related to conical cutter rock breaking. Sun carried out single-cutter breaking rock tests on limestone and basalt with the conical cutter and conventional cutter. They analyzed the effect of cutting angles and cutting depths on the rock-breaking efficiency (Sun et al., 2015). Pryhorovska established different rock-breaking models for different PDC cutters. Their findings revealed fluctuating cutting forces, suggesting no substantial difference between rotary cutting and linear cutting (Pryhorovska et al., 2015). Additionally, Xiong carried out a series of single-cutter tests on the granite with the conventional cutter and conical cutter. Their analysis focused on the effect of cutting angles, cutting depths, and cutting speeds on the efficiency of rock-breaking (Xiong et al., 2023a).

Several scholars have researched the cutting process by experimental and simulation. Pittino developed a computational method to simulate the process of rock-breaking, focusing on assessing the reaction force under different cutting parameters (Pittino et al., 2015). Cheng carried out a series of PDC cutter cutting tests. During the test, the cutting process was recorded with the camera. Their investigation further utilized thin-section optical microscopy to trace the development of cracks (Cheng et al., 2019).

The failure mode of rocks broken by PDC cutters is also an issue worthy of investigation. He investigated the failure mode of rock at different cutting depths (He et al., 2017). The researchers from the University of Pittsburgh established a single-cutter cutting model to investigate the transition of rock failure mode between ductile failure and brittle failure during the cutting tests (Zhou and Lin, 2014). Liu found that the brittle failure of rock would be suppressed with the increase of back rake angle (Liu et al., 2018). In addition, Dai found that the variation in cutting force could reflect the mode of rock failure (Dai et al., 2020). Xiong carried out a series

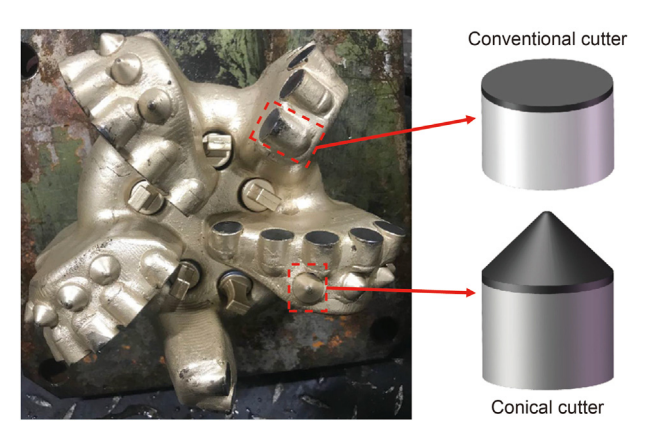


Fig. 1. Conventional cutter and conical cutter.

of single cutter tests of conical cutter under confining pressure, and analyzed the effects of confining pressure, cutting angle, cutting speed and cutting depth on cutting force. The numerical model was established to simulate cracks and damage in rock and the process of rock breakage (Xiong et al., 2023b).

The rock breaking characteristics and mechanism of conical cutter and conventional cutter are obviously different. Xiong carried out a series of mixed cutting tests using conical cutter and conventional cutter for granite. Combining the rock breaking characteristics of the two kinds of PDC cutters and giving full play to their respective advantages, the rock breaking laws under different cutting distribution parameters are analyzed (Xiong et al., 2022). Fu carried out a single cutter cutting tests with conical cutter and conventional cutter on carbonate rock. The differences of cutting groove morphology and cuttings distribution were compared between these two kinds of cutters (Fu et al., 2023).

The above investigations are mainly comparing the influence of cutting parameters, such as cutting angle and cutting depth, on conical cutter breaking different kinds of rocks. However, there are few studies on the detailed analysis of the process of cutting carbonate rocks with conical cutter and the relationship between the morphological characteristics of the cuttings and the failure mode of rock. Furthermore, most of the previous studies on the damage mode of rock are qualitatively analyzed and lack quantitative characterization.

In this study, a series of single-cutter cutting carbonate rock tests were conducted by conventional cutter and conical cutter. The characteristics of cutting carbonate rock are compared and analyzed in terms of cutting force, cutting process, and surface topography of rocks. Then, the calculation method for the brittle fracture index was established for quantitative characterization of fracture mode. The findings of this research will help to enhance the understanding of carbonate rock breakage characteristics and mechanism by conventional and conical cutter.

2. Experimental setup

2.1. Experimental equipment

These experiments were carried out by the single cutter cutting and rock-breaking device (Xiong et al., 2020a). As shown in Fig. 2(a), this device mainly consists of four components: the rock sample clamping system, cutting system, controlling system, and data acquisition system. The rock sample is fixed in the rock sample clamping system using threads. There are four long bolts on the cuttings holding device. The rock sample will be held in the clamping device of rock sample by tightening these four bolts. The cutting system is mainly driven by an electric motor, which can propel the horizontal bed along a guide rail. The moving speed of the horizontal bed is the cutting speed. The speed ranges from 1.6 to 230 mm/s. Notably, the horizontal bed can only realize linear movement along the guide rail. The main function of the control system is to set the cutting speed and cutting length. The cutting length is determined by the size of the rock samples. Typically, there are two sizes of rock samples, one is a cube of 150 mm \times 150 mm \times 150 mm and the other is a cube $100 \text{ mm} \times 100 \text{ mm} \times 100 \text{ mm}$. The data acquisition system is used to collect the cutting force data. The cutting force is the resistance of the cutter from the rock sample along the direction of movement. The core component of the data acquisition system is a load pressure sensor. The range of the load pressure sensor is 0~10 kN. The accuracy of measurement is 1.0 N. The maximum data acquisition frequency is up to 500 kHz. This equipment operates at a power of 2~3 kW approximately.



Fig. 2. Single cutter cutting and rock-breaking device (a); ST400 3D Profilometer (b).

The morphological characteristics of the cutting groove were acquired with the ST400 3D Profilometer (as shown in Fig. 2(b)). The ST400 3D Profilometer adopts the most advanced white light axial chromatic aberration technology to realize fast, high-resolution, and wide-ranging three-dimensional surface topography measurements. The minimum scanning step is 0.1 μm . The scanning speed reaches 20 mm/s. The scanning area can be set according to the actual size of the rock sample. Subsequently, the data regarding the depth and volume of the cutting groove can be acquired.

Fig. 3 shows the designed PDC cutter holders with different cutting angles according to the shapes of these two cutters. The cutter holders are available with cutting angles of 10° , 20° , 30° and 40° . The conical cutter is fixed to the holder using super glue. Whereas, the conventional cutter is fixed to the holder by tightening the screw, thus making the conventional cutter removable as well.

2.2. Experimental materials

In this paper, the conical cutter and conventional cutter widely used in oilfield drilling were selected to carry out the cutting tests. The two cutters are comprised of a diamond layer and a tungsten carbide (WC) stud.

The carbonate rock samples used in these tests were collected from Shaanxi Province, China. As shown in Fig. 4, they were machined into cubes of $100~\text{mm} \times 100~\text{mm} \times 100~\text{mm}$. And the mineral fractions of these carbonate rock samples were analyzed using X-ray diffraction (XRD). It mainly contains calcite, which accounts for 94%. In addition, the mechanical properties of carbonate

rock samples were measured and the results are shown in Table 1.

2.3. Experimental procedures

In this research, forty group cutting tests were carried out using conventional and conical cutters with different cutting angles and cutting depths. Previous research has indicated that the thickness of every layer of rock cut by a PDC cutter ranges between 1.0 and 3.0 mm (Raymond et al., 2012). Consequently, the cutting depths for the tests were set as 1.0, 1.5, 2.0, 2.5, and 3.0 mm, respectively. The cutting angle of the PDC cutter in previous cutting tests carried out by researchers remained below 40°. Hence, the cutting angles were set as 10°, 20°, 30°, 40°. Notably, scholars have confirmed that the cutting speed ranging between 5 and 25 mm/s has little effect on the cutting force (Xiong et al., 2023a). Therefore, the cutting speed was set as 5 mm/s. The cutting length was determined as 230 mm. The experimental scheme is shown in Table 2.

Firstly, a relatively flat rock surface was selected as the cutting surface to ensure that the cutting depth is consistent throughout the cutting process. The rock sample was then placed within the rock sample clamping system, firmly fixed in place by tightening the bolts. Secondly, the cutting depth was adjusted by the micrometer in Fig. 2(a). Thirdly, the cutting speed and cutting length were set by the controlling system. Then the data acquisition system and test system were turned on and running. Here, the data acquisition frequency was set as 500 Hz. During the cutting process, the high-speed camera was used to record the cutting process. After cutting tests, the morphology of cutting grooves was reconstructed with the ST400 3D Profilometer. Meanwhile, the data on the depth and area of the cutting grooves will also be acquired.

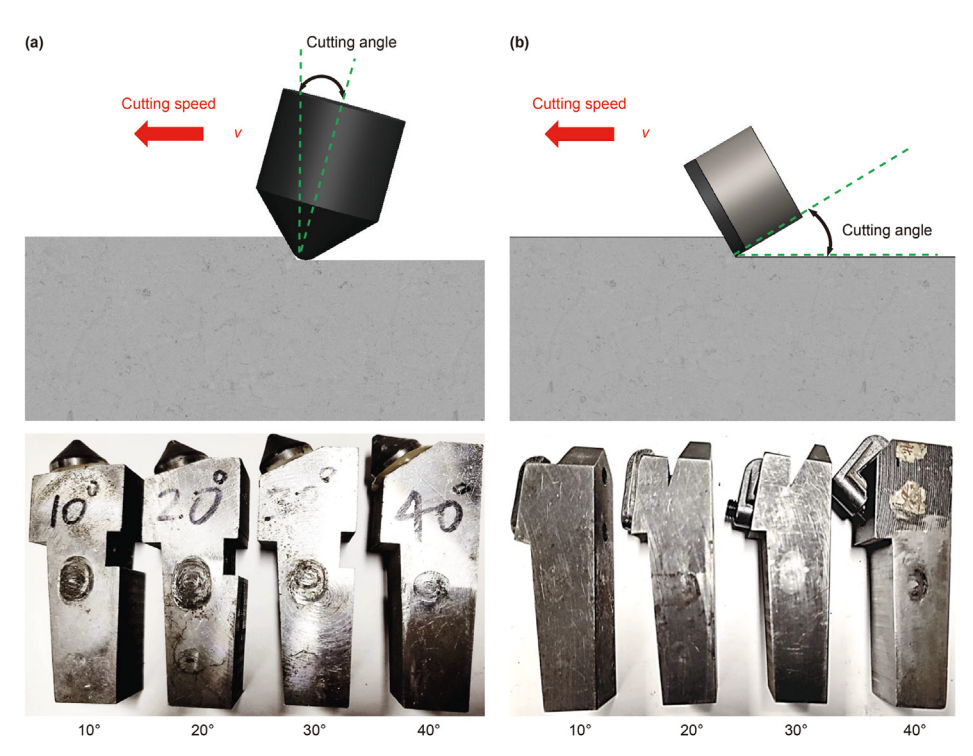


Fig. 3. Conical cutter holders (a) and conventional cutter holders (b) under different cutting angles.

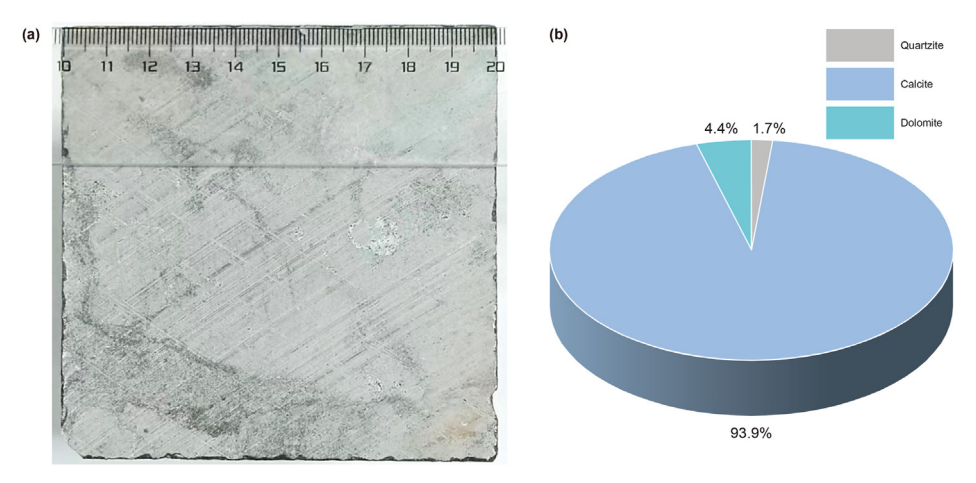


Fig. 4. Carbonate rock sample (a); mineral composition of carbonate rock (b).

Table 1The mechanical properties of rock samples.

| Density, g/cm ³ | Young's modulus, GPa | Poison's ratio | Cohesive strength, MPa | Internal friction angle , $^{\circ}$ | UCS, MPa | Tensile strength, MPa |
|----------------------------|----------------------|----------------|------------------------|--------------------------------------|----------|-----------------------|
| 2.70 | 66 | 0.24 | 59.59 | 32.27 | 187 | 8.66 |

3. Experimental results

3.1. Cutting force characteristics

The cutting force can reflect the characteristics of cutting process. As is shown in Fig. 5, the average cutting force at different cutting depths and cutting angles was calculated. It is clearly shown that the average cutting force of conventional cutter and conical

cutter increases with the increase of cutting depth. This is because the contact area between the PDC cutter and the rock increases with the increase of cutting depth. The interaction between the PDC cutter and the rock is enhanced. Therefore, the average cutting force increases. At the same cutting depths, the average cutting force of conventional cutter shows an increase corresponding to the increase of cutting angle. Whereas, the average cutting force of the conventional cutter is approximately the same at different cutting

Table 2 The experiment schemes.

| Type of cutter | Cutting angle, ° | Cutting depth, mm | |
|---------------------|------------------|---------------------|--|
| Conventional cutter | 10 | 1.0/1.5/2.0/2.5/3.0 | |
| | 20 | 1.0/1.5/2.0/2.5/3.0 | |
| | 30 | 1.0/1.5/2.0/2.5/3.0 | |
| | 40 | 1.0/1.5/2.0/2.5/3.0 | |
| Conical cutter | 10 | 1.0/1.5/2.0/2.5/3.0 | |
| | 20 | 1.0/1.5/2.0/2.5/3.0 | |
| | 30 | 1.0/1.5/2.0/2.5/3.0 | |
| | 40 | 1.0/1.5/2.0/2.5/3.0 | |

angles when the cutting depth is 1.0 mm. Because the contact area between the conventional cutter and the rock is minimal. The contact area between the conventional cutter and the rock is approximately the same when the cutting depth is 1.0 mm. Similarly, the average cutting force of the conical cutter is approximately the same when the cutting depth is 1.0 mm. The reason is the same as that of the conventional cutter. The contact area between the conical cutter and the rock is approximately the same when the cutting depth is 1.0 mm.

Fig. 6 shows the variation of cutting force with cutting time at the cutting depth of 1.0 and 3.0 mm. The variation of cutting force of conventional cutter and conical cutter is similar at the cutting depth of 1.0 mm. The average cutting force of conventional cutter is 332.49 N. The average cutting force of the conical cutter is 311.88 N. The average cutting force of these two cutters is the same roughly. Whereas, the average cutting force of the conventional cutter is larger than that of the conical cutter obviously at the cutting depth

of 3.0 mm. The average cutting force of the conventional cutter is 823.37 N. In comparison, the average cutting force of the conical cutter is 635.89 N. The interaction area between these two cutters and the rock is different due to the different shapes of these two cutters. The contact area between the conventional cutter and rock is larger than that between the conical cutter and rock with the increase of cutting depth (Xiong et al., 2020b). The interaction between the conventional cutter and rock is stronger than that between the conical cutter and rock obviously.

In addition, an interesting thing is that the standard deviation of the cutting force of the conventional cutter at the cutting depth of 1.0 mm is 96.56. The standard deviation of the cutting force of the conventional cutter at the cutting depth of 3.0 mm is 432.32. However, the standard deviation of the cutting force of the conical cutter at the cutting depth of 1.0 mm is 83.21. The standard deviation of the cutting force of the conical cutter at the cutting depth of 3.0 mm is 224.59. The standard deviation data shows that the increase in cutting depth leads to an increase in the fluctuation degree of the cutting force. Especially, the cutting force of the conventional cutter is more sensitive to the increase in cutting depth. As is shown in Fig. 6(b), large cutting intervals appear intermittently in the cutting force curve of the conventional cutter at the cutting depth of 3.0 mm.

Based on the previous analysis, the cutting force curve exhibits an alternating state of ascent and descent. Therefore, the cutting force curve can be divided into the loading stage and the failure stage (Dai et al., 2021a). As is shown in Fig. 7, the cutting force can be divided into loading stage AD and failure stage DE. Indeed, a small drop of cutting force BC appears in the loading stage due to

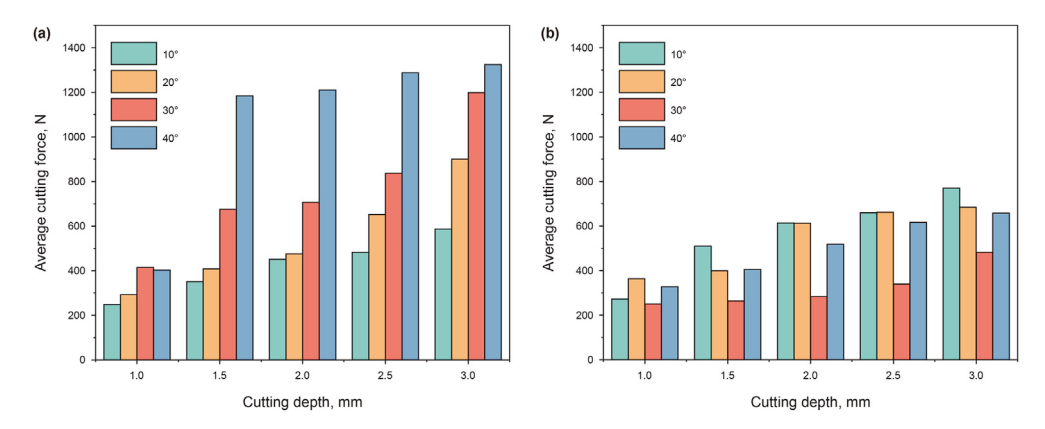


Fig. 5. The average cutting force at different cutting angles and depths: (a) conventional cutter, (b) conical cutter.

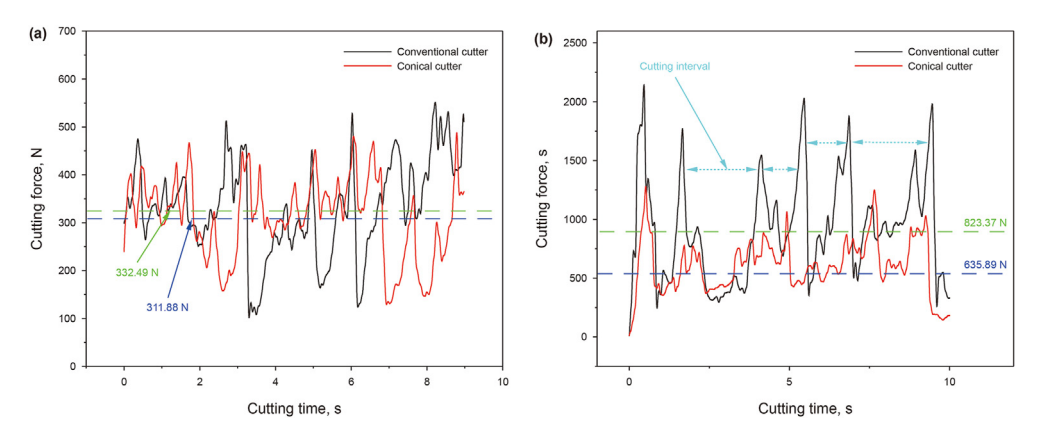


Fig. 6. Variation of cutting force with cutting time ((a) cutting depth: 1.0 mm; (b) cutting depth: 3.0 mm).

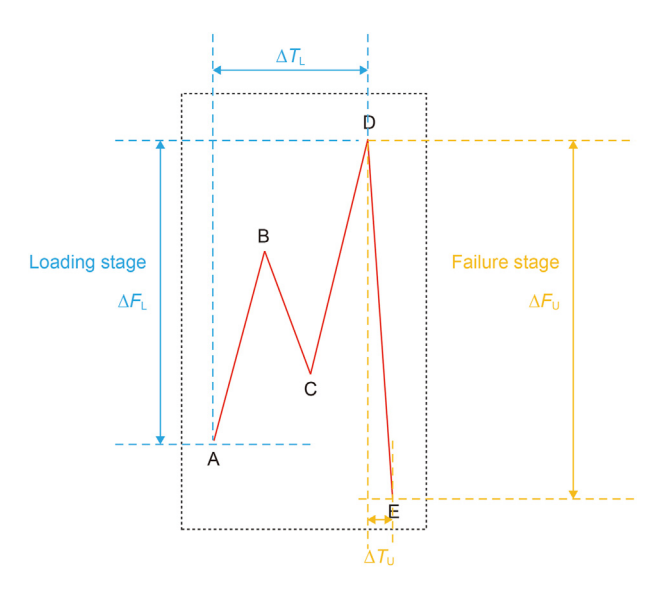


Fig. 7. Loading stage and failure stage of cutting force.

the localized fracture of the rock. But this drop stage BC is smaller than the value of the failure stage. And the small increase stage CD is smaller than the value of the loading stage. Therefore, we ignore the drop stage BC and increase stage CD during the process of counting the loading stage and failure stage. The cutting force difference and the corresponding cutting time difference in the loading stage and failure stage were calculated respectively to analyze the changing trend of cutting force in the loading stage and failure stage. To describe the variation rate of cutting force difference, the variation rate of cutting force difference was defined. The calculation method can be expressed as (Dai et al., 2020):

$$V_F = \frac{\Delta F}{1000*\Delta T} \tag{1}$$

where, V_F is the variation rate of cutting force difference, kN/s; ΔF is the cutting force difference, N; ΔF_L is the cutting force difference of loading stage, N; ΔF_U is the cutting force difference of failure stage, N; ΔT is the cutting time difference, s; ΔT_L is the cutting time difference of loading stage, s; ΔT_U is the cutting time difference of failure stage, s.

As is shown in Fig. 8(a), the variation rate of cutting force difference during the rock loading stage of the conventional cutter ranges between 1 and 4 kN/s. Interestingly, the variation rate of cutting force difference has little relation with the difference of

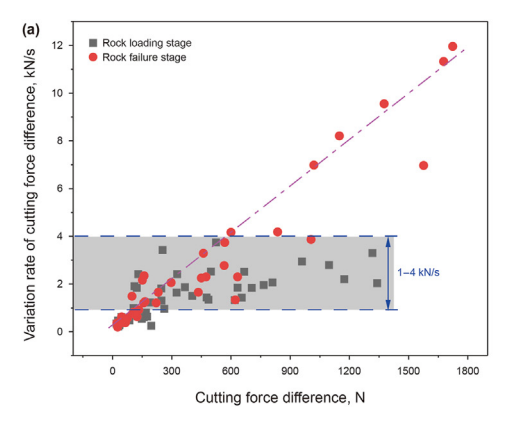
cutting force. Conversely, the variation rate of cutting force difference during the rock failure stage of the conventional cutter grows linearly with the cutting force difference. This shows that the loading stage of the conventional cutter on the rock is homogeneous. However, based on the data for cutting force difference and the corresponding cutting time difference, when the cutting force difference decreases sharply, the corresponding cutting time difference remains within a relatively short period. Consequently, the calculation results of V_F show a gradual increase in the value of V_F , as illustrated by the red oblique line in Fig. 8(a). The attenuation process of the cutting force, referred to as the rock failure stage above, is an instantaneous process. This also indicates that carbonate rock is relatively brittle.

As shown in Fig. 8(b), the variation rate of the cutting force difference of the conical cutter with cutting force difference is significantly different from that of conventional cutter. During the rock loading stage and rock failure stage, the variation rate of cutting force difference is basically below 3 kN/s. Additionally, the cutting force difference of the rock loading stage and the failure stage of the conical cutter is below 900 N. In contrast, the cutting force difference of the rock loading stage and the failure stage of the conventional cutter is below 1800 N. This distinction shows that the rock loading stage and failure stage of the conical cutter occur within a brief duration. Moreover, the degree of fluctuation in the cutting force for the conical cutter is comparatively lower than that of the conventional cutter. The cutting process of the conical cutter is more stable.

There is a common interesting phenomenon in the cutting process of conical cutter and conventional cutter. The cutting force difference during the loading stage is consistently lower than that of the failure stage. The distribution of data points of variation rate of cutting force difference during the loading stage is more concentrated than that of cutting force difference during the failure stage. This observation suggests a continuous nature of the rock failure stage. During a single rock failure stage, the cutting force is reduced directly from a larger value to a minimum value without secondary reduction. As is shown in Fig. 7, during the loading stage, there is a process of decrease and then increase in the cutting force curve, leading to a discontinuous nature of the loading stage. Conversely, the failure stage is almost always continuous. Hence, the cutting force difference during the failure stage is greater than that of the loading stage.

3.2. Rock breakage process

Capturing the process of cutting test can help to observe the damage details of the carbonate rock. The high-speed camera was



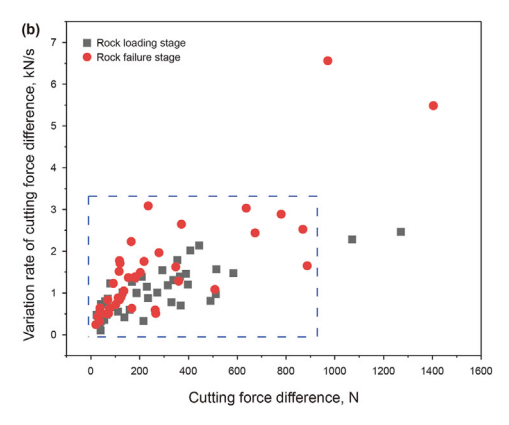


Fig. 8. Variation rate of cutting force difference with cutting force difference ((a) conventional cutter; (b) conical cutter).

used to record the cutting process of these two cutters, followed by frame extraction from the video at the rate of 60 frames per second. The cutting process of conventional cutter and conical cutter are shown in Figs. 9 and 10 respectively.

As is shown in Fig. 9, the conventional cutter causes compaction to the rock in front of the cutter during the process of cutting carbonate rock with the conventional cutter. With the continuous advancement of the conventional cutter in the cutting direction. the interaction between the cutter and rock is enhanced, occasionally resulting in sporadic splashes of small particles. When the interaction between the cutter and rock is enhanced to the strength of the rock, the rock in front of the cutter is failure and large amounts of particles are released. This is consistent with the previous analysis of the cutting force. With the continued enhancement of the interaction between cutter and rock, the cutting force increases. When the bursting of a small particle occurs, the cutting force decreases briefly and then continues to increase until the interaction between the cutter and rock reaches the rock strength and the rock in front of the cutter is failure. With the removal of large amounts of rock debris, the interaction between the cutter and rock is broken, causing a rapid decline in cutting force.

The process of cutting carbonate rock with the conical cutter is different from that of the conventional cutter. As is shown in Fig. 10, during the process of cutting carbonate rock with the conical cutter, with the continuous advancement of the cutter along the cutting direction, the rock in front of the cutter is constantly destroyed and then bursts due to the interaction from the cutter. Consequently, there is a continuous burst of small particles of rock debris in front of the cutter. As shown in Fig. 10(f), there is a large rock debris splash in front of the conical cutter.

The energy accumulated between the PDC cutter and the rock gradually increases during the interaction process. Simultaneously, the cutting force also increases gradually. However, the burst of rock debris in front of the cutter weakens the accumulated energy between the cutter and the rock. The cutting force decreases subsequently. In the process of interaction between the conventional cutter and rock, there is an obvious compaction stage in the cutting process. This stage is characterized by the absence of bursting rock debris in front of the cutter. As shown in Fig. 11(a), the accumulation of rock debris in front of the conventional cutter enhances the interaction between the conventional cutter and the rock. However, in the process of interaction between the conical cutter and the rock, the rock debris in front of the cutter burst out constantly. The rock debris slides over the sides of the conical cutter basically (as shown in Fig. 11(b)). Consequently, the energy accumulated between the conical cutter and the rock is constantly released,

explaining the lower average cutting force exerted by the conical cutter compared to the conventional cutter.

In fact, the entire cutting process of the conventional and conical cutters is exactly the rock-breaking process in Figs. 9 and 10 repeated continuously. Based on the recorded video from the cutting test with both types of cutters, the precise moments of each large amounts of rock debris burst were captured. Calculating the time difference between successive occurrences of these significant bursts allowed us to illustrate the time intervals between them, as shown in Fig. 12. It can be intuitively demonstrated that the time difference between the two adjacent bursts of large amounts of rock debris during the process of cutting rock by the conventional cutter is longer than that of conical cutter. As shown in Fig. 6(b), there are several cutting force intervals in the cutting force curve of the conventional cutter. The cutting force interval corresponds to the moments when large amounts of rock debris burst out, leading to an instantaneous decrease in the interaction between the conventional cutter and the rock. Consequently, this causes a sharp decline in the cutting force, marking these intervals with relatively low force values.

Certainly, there are errors in the experiment, including those from processing the test videos. Additionally, the samples used in the experiment are natural rocks with significant heterogeneity. As a result, there are instances where the time intervals between large debris bursts during cutting with the conical cutter are greater than those with the conventional cutter.

3.3. Surface morphology of cutting grooves

The cutting grooves produced by the PDC cutter can also reflect the cutting characteristics of the PDC cutter. The characteristics of cutting grooves at different cutting depths are significantly different. Fig. 13 shows the cutting grooves produced by the conventional and conical cutters at the cutting depths of 1.0 and 3.0 mm.

At the cutting depth of 1.0 mm, there are compacted cuttings at the bottom of the cutting groove produced by the conventional and conical cutters, resulting from the compressive action of the PDC cutter on the cuttings under the cutter. However, the difference is that the compacted cuttings at the bottom of the cutting groove produced by the conventional cutter are intermittent and wide. Whereas, the compacted cuttings at the bottom of the cutting groove produced by the conical cutter are continuous and narrow. In addition, the cutting groove produced by the conical cutter is surrounded by small blocky debris. However, the cutting grooves produced by the conventional cutter are surrounded by granular cuttings.

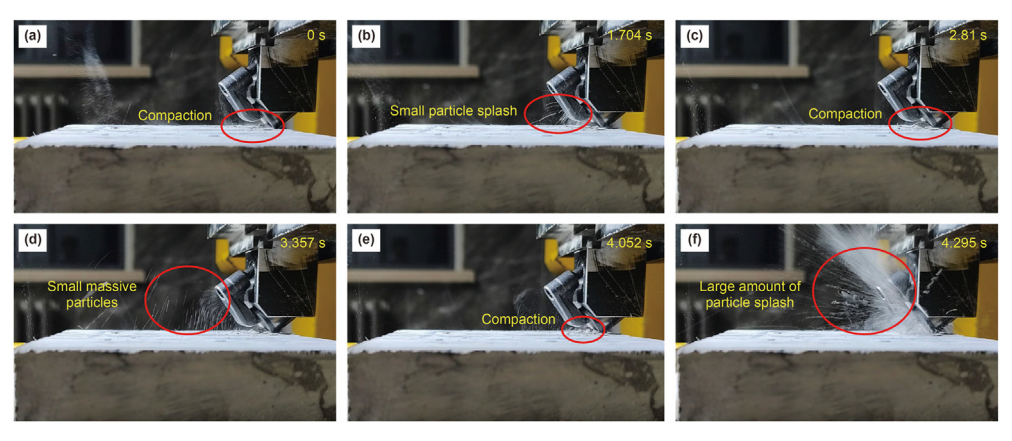


Fig. 9. A typical process of a conventional cutter breaking carbonate rock.

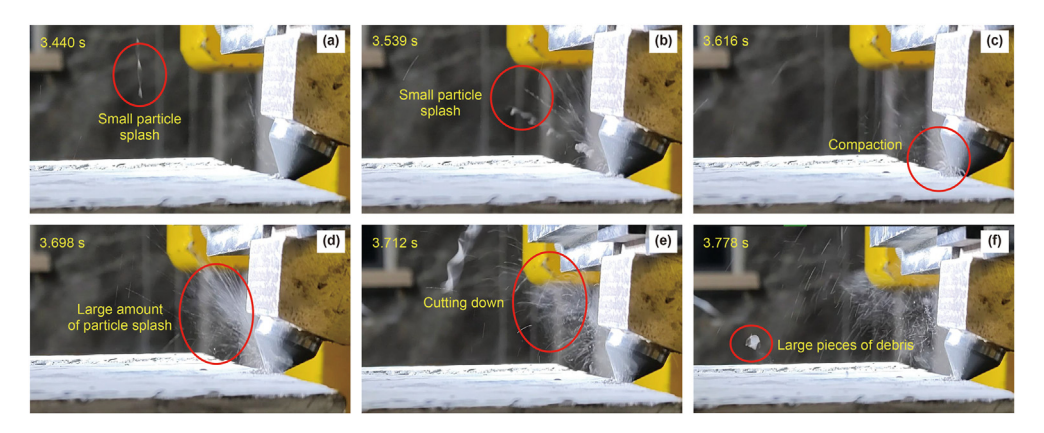


Fig. 10. A typical process of a conical cutter breaking carbonate rock.

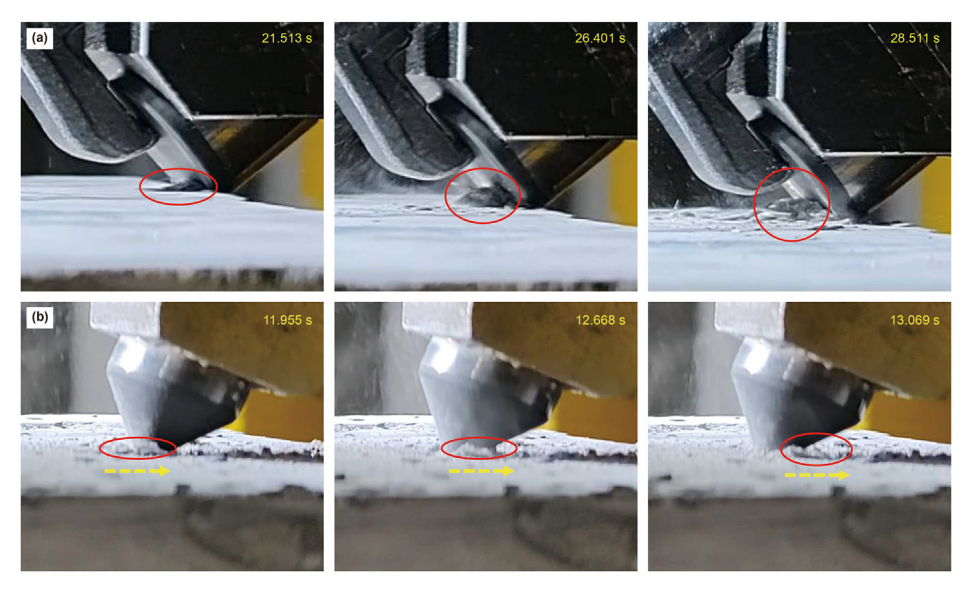


Fig. 11. The process of cuttings accumulation in front of a conventional cutter (a). The process of cuttings sliding over the sides of the conical cutter (b).

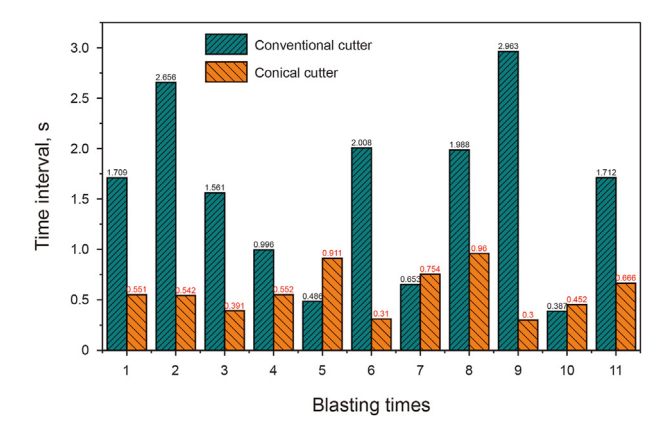


Fig. 12. Time interval statistics for each blast during the cutting process.

At the cutting depth of 3.0 mm, the cutting grooves produced by the conventional and conical cutters are covered with cuttings. It can be observed that the cutting groove produced by the conical cutter is distributed with blocky rock debris of different shapes and sizes. However, the number of blocky rock debris distributed in the

cutting groove produced by the conventional cutter is less, which may be splashed out by the burst.

The morphology of the cutting groove provides insights into the fracture mode of carbonate rock. The cuttings covered by the cutting groove were cleaned, and then the morphological characteristics of the cutting groove produced by the conventional and conical cutters at the cutting depth of 1.0 and 3.0 mm were obtained by the ST400 3D Profilometer. Fig. 14 shows the morphology of cutting groove produced by these two cutters at the cutting depth of 1.0 and 3.0 mm. The morphology characteristics of cutting grooves produced by the conventional cutter and the conical cutter at different cutting depths are significantly different.

At the cutting depth of 1.0 mm, the two sides of the cutting groove produced by the conical cutter are distributed with irregular, jagged tensile damage zones. The bottom of the cutting groove is distributed with a narrow compressive damage zone. In contrast, the contours of both sides of the cutting groove produced by the conventional cutter are relatively flat. The failure mode of the rock is mainly plastic damage with conventional cutter.

At the cutting depth of 3.0 mm, the difference from the cutting groove at the cutting depth of 1.0 mm is that the bottom of the cutting groove produced by the conventional cutter is uneven and distributed with intermittent compressive damage zones. In

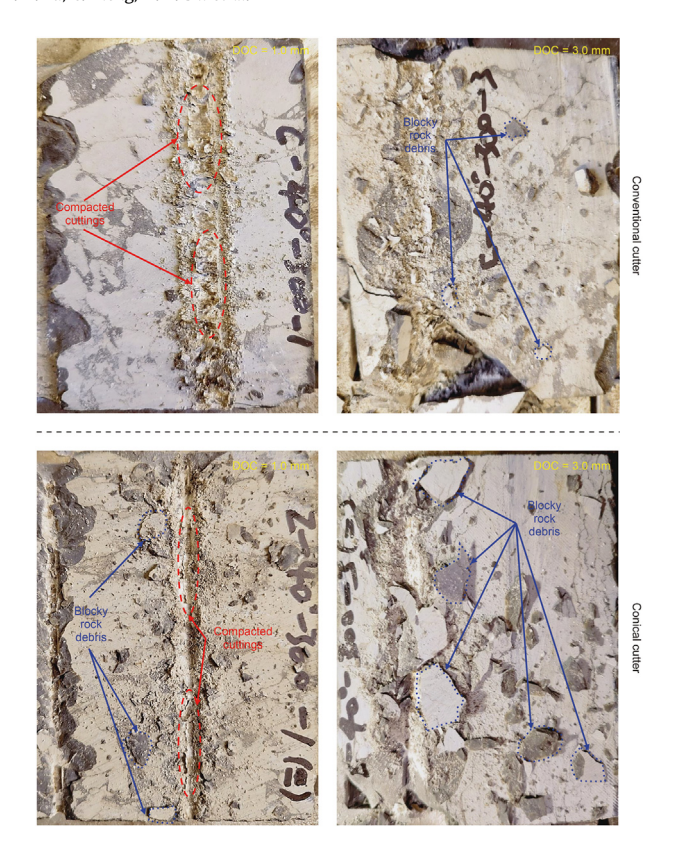


Fig. 13. The cutting groove produced by conventional cutter and conical cutter at the cutting depth of 1.0 and 3.0 mm (DOC: cutting depth).

addition, symmetrical fan-shaped brittle tensile damage zones are distributed on both sides of the cutting groove. Conversely, the characteristics of the cutting groove produced by the conical cutter

are different from those of the conventional cutter. The similarities with the cutting groove at the cutting depth of 1.0 mm are the continuous plastic compressive damage zone at the bottom of the cutting groove accompanied by the asymmetric jagged tensile brittle damage zones on both sides of the cutting groove.

The fracture of rock on both sides of the conical cutter is randomly distributed due to the presence of calcite joints. The cleavage of calcite is naturally arranged in an orderly manner. The cuttings on the fracture surface tends to be broken on both sides along the direction of the interaction force of the conical cutter. In addition, different from the conventional cutter, the cutting surface of the conical cutter is a smooth surface without sharp edges. This results in the lack of the trimming effect of sharp edges on both sides of the cutting groove. This explains the irregular distribution of the jagged fracture zones on both sides of the cutting groove produced by the conical cutter. In contrast, the sharp edges of the conventional cutter have a trimming effect on the cutting groove. Therefore, the contours on both sides of the cutting groove are relatively flat when the cutting depth is 1.0 mm. However, when the cutting depth is 3.0 mm, there are obvious brittle fracture zones on both sides of the cutting groove of conventional and conical cutter. Because the brittle fracture caused by the cutter increases with the increase of cutting depth (Liu et al., 2018).

3.4. Cuttings characteristics

From the above analysis, it is evident that blocky rock debris and granular cuttings are produced during the cutting process of the conventional and conical cutters. The morphological characteristics of blocky rock debris can reflect the mode of rock damage. Fig. 15 shows the morphology of blocky rock debris generated by the conventional and conical cutters. In addition, the cross-section height of the cuttings in the cutting direction can be obtained from the data measured by the ST400 3D Profilometer. Fig. 16 shows the distribution of cuttings height.

As shown in Figs. 15 and 16, the height of the cuttings generated

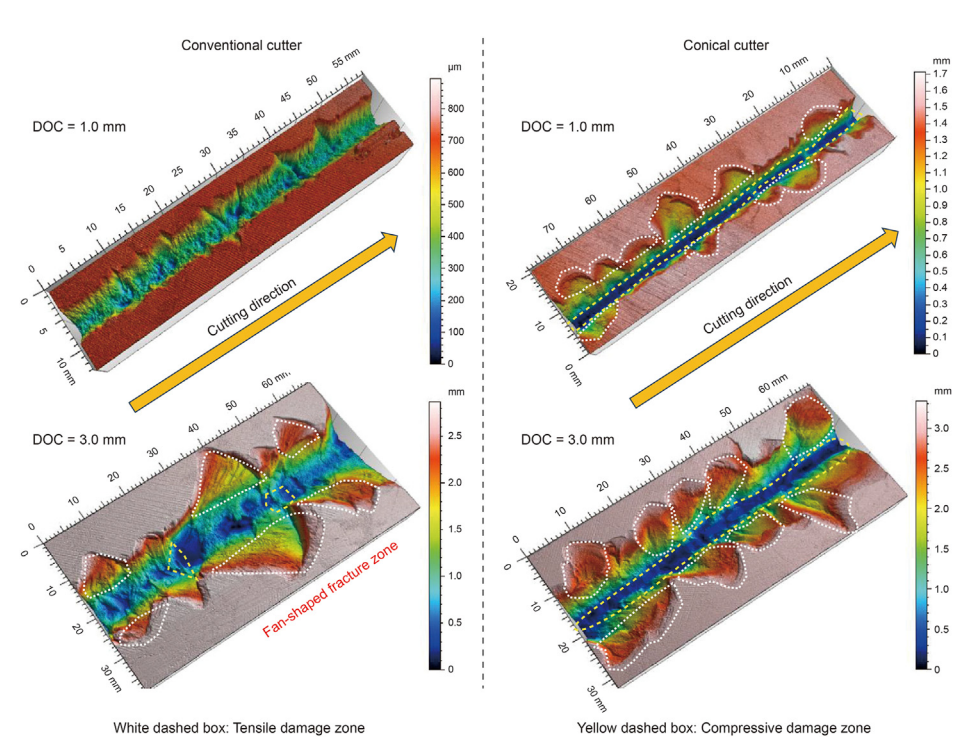


Fig. 14. The fracture mode of cutting groove of conventional cutter and conical cutter.

by the conventional cutter and conical cutter is gradually reduced along the cutting direction. The height of cuttings is highest at the starting position of the cutting direction, indicating a gradual decrease in the stress on the rock under the cutter from the position near the cutter to the distant location. Another interesting thing is that the height of the rock cuttings generated by the conical cutter is 0.5 mm higher than that of rock cuttings generated by the conventional cutter, indicating a higher concentration of the stress under the conical cutter. Furthermore, the surface of the cuttings generated by the conical cutter appears smoother, resembling a scallop. Whereas, the surface of the cuttings generated by the conventional cutter is uneven and shows stepped.

3.5. Quantitative characterization of fracture mode

According to the above analysis, the conventional cutter and conical cutter cause different degrees of brittle tensile damage to the rock. At the same cutting conditions, the larger the brittle fracture area, the better the effect of breaking rock. How to evaluate the degree of brittle fracture quantitatively will become meaningful. The brittle fracture index was calculated to reflect the degree of brittle fracture. The brittle fracture index is defined as the ratio of real breaking rock volume to the theoretical plastic breaking rock volume (Dai et al., 2021b). Therefore, the larger the brittle fracture index, the better the effect of breaking rock. The calculation formula for the brittle fracture index is as follows:

$$Index_b = \frac{V_{real}}{V_{plastic}} \tag{2}$$

where, $Index_b$ is the brittle fracture index; V_{real} is the volume of real cutting groove, mm³; $V_{plastic}$ is the volume of theoretical plastic deformation zone, mm³.

The measurement of the actual volume of the cutting groove $V_{\rm real}$ and the calculation of the volume of plastic deformation zone $V_{\rm plastic}$ are based on the same cutting length. Therefore, we only need to calculate the cross-sectional area of the real cutting groove and the cross-sectional area of the plastic deformation zone. Then Eq. (2) can thus be simplified as follows:

$$Index_b = \frac{S_{real}}{S_{plastic}} \tag{3}$$

where, $S_{\rm real}$ is the area of the cross-sectional zone of real cutting groove, mm². In the previous study, we mentioned that the morphology of the cutting groove was obtained with the ST400 3D Profilometer. The volume and length of the cutting groove can also be obtained. To be specific, the data of three-dimensional coordinates of the cutting groove can be obtained with the ST400 3D Profilometer. Based on the data of the three dimensions coordinate,

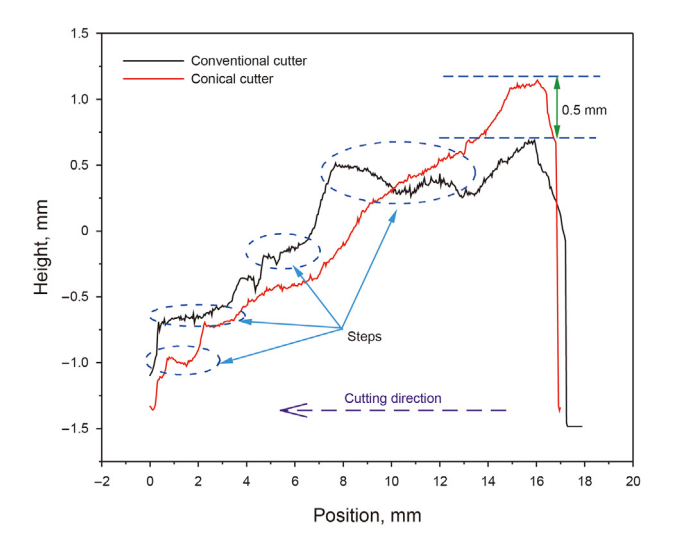


Fig. 16. The distribution of cuttings height.

the volume of the cutting groove can be calculated by the postprocessing software of the equipment. Consequently, the average cross-sectional area of the cutting groove is derived by dividing the volume of the cutting groove by the length of the cutting groove.

 $S_{
m plastic}$ is the area of the cross-sectional zone of theoretical plastic deformation zone, mm². The theoretical plastic deformation zones of these two cutters are different significantly due to the different shapes of the cutters.

Firstly, we calculate the area of the cross-sectional zone of the theoretical plastic deformation zone produced by the conventional cutter. As is shown in Fig. 17, the solid yellow area is the interaction area between the conventional cutter and the rock. The area of this section needs to be calculated, which is shown in the blue rectangular dotted box.

$$d_{x} = d \cdot \sec \alpha \tag{4}$$

where, d is the cutting depth, mm; α is the cutting angle of the conventional cutter, $^{\circ}$.

The angle between line OA and line OB is defined as β , which can be calculated as follows:

$$\beta = \arccos\left(\frac{OA}{OB}\right) = \arccos\left(\frac{r - d_x}{r}\right) = \arccos\left(\frac{r - d \cdot \sec \alpha}{r}\right)$$
(5)

where, r is the diameter of the conventional cutter, mm. It is a constant value, of 8.0 mm.

Then the area of the solid yellow area can be calculated as

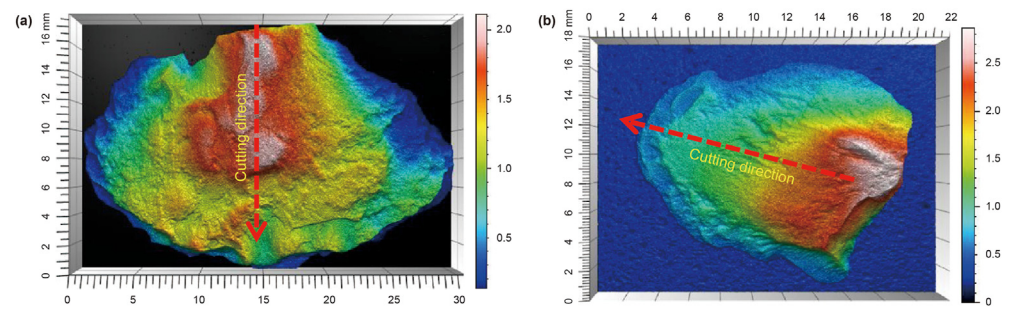


Fig. 15. The morphology of the cuttings ((a)) produced by conventional cutter; (b) produced by conical cutter).

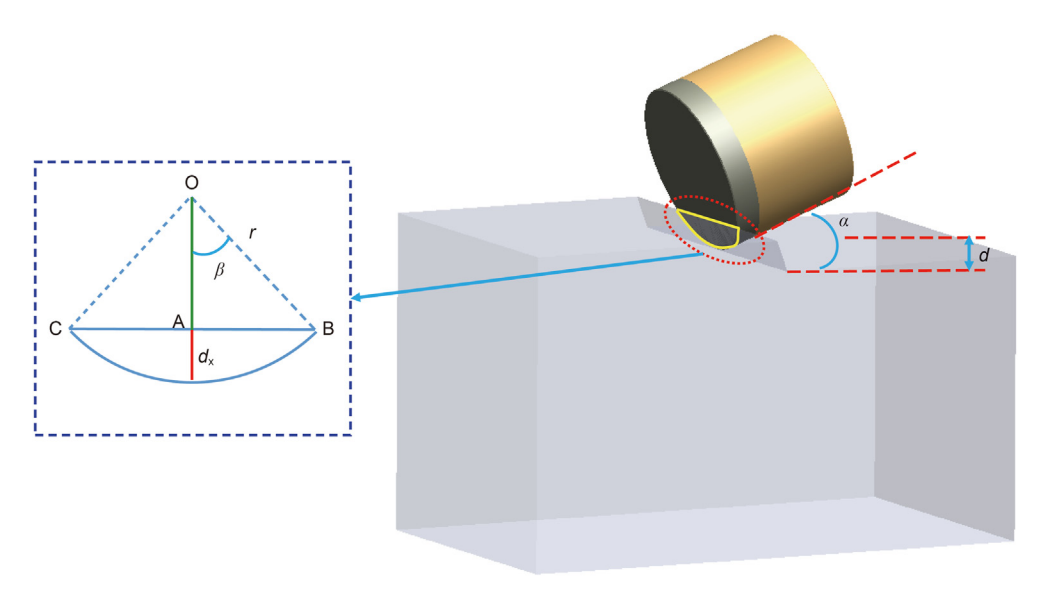


Fig. 17. The sketch of the cross-sectional area of the plastic deformation zone produced by the conventional cutter.

follows:

$$S_{\text{vellow}} = 0.5 \cdot 2\beta \cdot r^2 - 2 \cdot 0.5 \cdot (r - d \cdot \sec \alpha) \cdot r \cdot \sin \beta$$
 (6)

Eq. (6) can be simplified as follows:

$$S_{\text{vellow}} = \beta \cdot r^2 - (r - d \cdot \sec \alpha) \cdot r \cdot \sin \beta \tag{7}$$

where,
$$\sin \beta = \frac{\sqrt{2 \cdot r \cdot d \cdot \sec \alpha - (d \cdot \sec \alpha)^2}}{2 \cdot r \cdot d \cdot \sec \alpha - (d \cdot \sec \alpha)^2}$$

Due to the existence of the cutting angle, the area of the solid yellow area is not the area of the cross-sectional zone of the plastic deformation zone, the area of the cross-sectional zone of the plastic deformation zone can be calculated as follows:

$$S_{\text{plastic}} = S_{\text{yellow}} \cdot \cos \alpha \tag{8}$$

According to Eqs. (5), (7) and (8), the equation for $S_{plastic}$ can be as follows:

Secondly, we calculate the plastic deformation zone produced by the conical cutter. It is essential to calculate the area of triangle CAB, which is shown in the blue rectangular dotted box (as shown in Fig. 18).

$$d_{\mathsf{x}} = d \cdot \sec \alpha \tag{11}$$

where, d is the cutting depth, mm; α is the cutting angle of the conical cutter, $^{\circ}$.

The cone tip angle of the conical cutter used in this test is 90° , thus the angle CAB is 90° . Then the area of triangle CAB will be calculated.

$$S_{\Delta ABC} = d_x^2 \tag{12}$$

Substitute Eq. (11) into Eq. (12) to derive the calculation equation for $S_{\Delta ABC}$. In fact, due to the existence of cutting angle α , the area of the solid blue area is not the area of the cross-sectional area of the plastic deformation zone. Therefore, the real cross-sectional

$$S_{\text{plastic}} = \left(\arccos\left(\frac{r - d \cdot \sec \alpha}{r}\right) \cdot r^2 - (r - d \cdot \sec \alpha) \cdot \sqrt{2 \cdot r \cdot d \cdot \sec \alpha - (d \cdot \sec \alpha)^2}\right) \cdot \cos \alpha \tag{9}$$

Subsequently, substitute Eq. (9) into Eq. (3) to derive the ultimate equation for the brittle fracture index applicable to rock-breaking process of the conventional cutter:

area of the plastic deformation zone can be calculated as follows:

$$S_{\text{plastic}} = d^2 \cdot \sec \alpha \tag{13}$$

$$Index_{b} = \frac{S_{real}}{\left(\arccos\left(\frac{r - d \cdot \sec \alpha}{r}\right) \cdot r^{2} - (r - d \cdot \sec \alpha) \cdot \sqrt{2 \cdot r \cdot d \cdot \sec \alpha - (d \cdot \sec \alpha)^{2}}\right) \cdot \cos \alpha}$$
(10)

Then substitute Eq. (13) into Eq. (3) to get the final equation for the brittle fracture index applicable to rock-breaking process of the

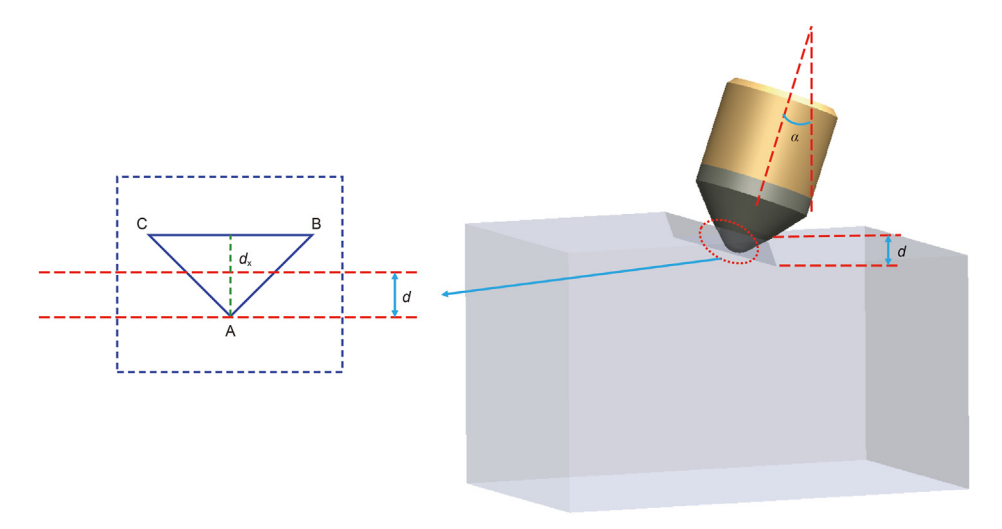


Fig. 18. The sketch of the cross-sectional area of the plastic deformation zone produced by the conical cutter.

conical cutter:

$$Index_{b} = \frac{S_{\text{real}}}{d^{2} \cdot \sec \alpha}$$
 (14)

Based on Eqs. (10) and (14), the variation of the area of the plastic deformation zone produced by these two cutters at different cutting angles and cutting depths is shown in Fig. 19(a) and (b). At the same cutting angle, the area of plastic deformation zone produced by these two cutters increases with the increase of cutting depth. Similarly, at the same cutting depth, the area of plastic deformation zone caused by these two cutters increases with the increase of cutting angle. Furthermore, the area of the cross-section of the plastic deformation zone produced by the conventional cutter is greater than that of the conical cutter at the same cutting angles and cutting depths. This also explains that the average cutting force of conventional cutter is greater than that of conical cutter. During the cutting process of the conventional cutter, there is an accumulation of rock debris in front of the conventional cutter. Meanwhile, the conical cutter has a weaker ability to cover the rock at the bottom of the well.

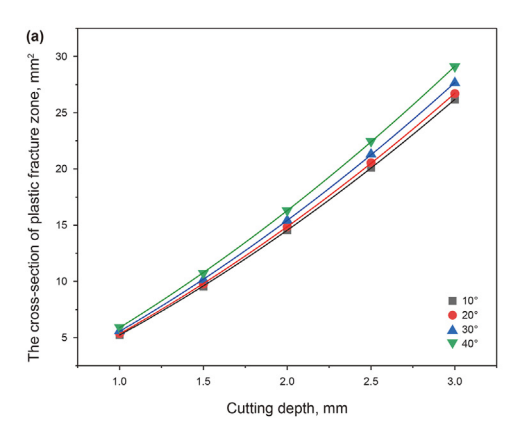
The variation of brittle fracture index for conventional cutter and conical cutter breaking rock under different cutting conditions are shown in Fig. 20(a) and (b) respectively. It can be found that the brittle fracture index of the conical cutter is two or three times larger than that of the conventional cutter. For carbonate rock, the

brittle fracture effect of the conical cutter is more obvious. The brittle fracture index of the conical cutter breaking rock is higher than that of conventional cutter obviously at the same cutting conditions. The conical cutter can better utilize the brittle fracture capacity when breaking carbonate rock.

Furthermore, the brittle fracture index of the conventional cutter at the cutting depth of 1.5 mm is larger than the brittle fracture index at the cutting depth of 1.0 mm under the cutting angles of 10° and 20°. It indicates that the brittle fracture ability of the conventional cutter at the cutting depth of 1.5 mm is stronger than that of conventional cutter at the cutting depth of 1.0 mm under these cutting angles. Notably, the brittle fracture index of the conventional cutter decreases with the increase of cutting angle at the cutting depths of 1.0 and 1.5 mm. Whereas, the brittle fracture index of conical cutter under the cutting angle of 20° is largest at the cutting depth of 1.0 mm. The brittle fracture index of conical cutter under the cutting angle of 40° is larger than that of conical cutter under the cutting angle of 20° at the cutting depth of 1.5 mm. However, considering the manufacturing process of PDC bit, the cutting angle of 20° is recommended.

4. Conclusions and suggestions

In this paper, a series of single cutter cutting carbonate rock tests with conventional cutter and conical cutter were carried out. The



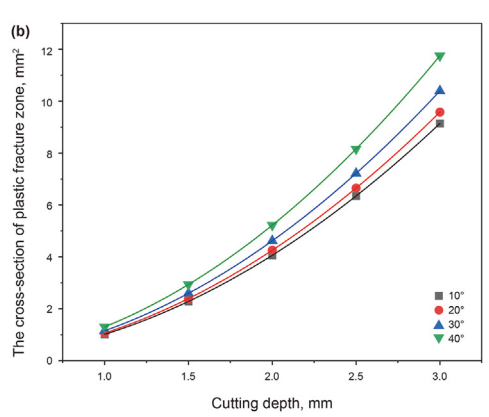
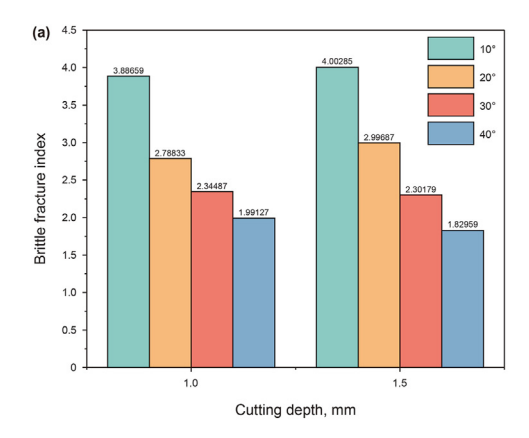


Fig. 19. The variation of the cross-section area of the plastic deformation zone produced by these two cutters versus cutting depths at different cutting angles. (a) conventional cutter, (b) conical cutter.



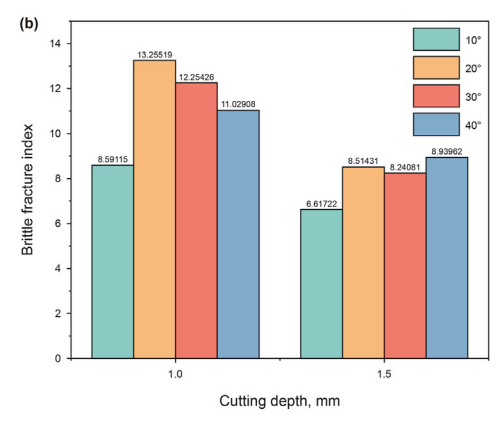


Fig. 20. Variation of brittle fracture index of conventional cutter (a) and conical cutter (b) breaking rock versus cutting angles at different cutting depths.

cutting force, rock breakage process, and characteristics of cutting grooves and cuttings were analyzed. In addition, the calculation for the brittle fracture index for these PDC cutters was established respectively. Subsequently, the brittle fracture index for these cutters under different cutting conditions was calculated. The breakage mode of carbonate rock cutting by conventional and conical cutters was determined. The major conclusions are as follows.

- (1) The average cutting force of conical cutter is less than that of conventional cutter. At the cutting depth of 3.0 mm, there are distinct cutting intervals during the cutting process of the conventional cutter. However, the cutting force curve of the conical cutter has no obvious cutting intervals, indicating a more stable cutting process.
- (2) The conventional cutter interacts with a larger area of the rock surface compared to the conical cutter. The stress exerted by the conventional cutter on the rock ahead is more dispersed, resulting in prolonged interaction time. In contrast, the stress on the rock exerted by the conical cutter is more concentrated, causing quicker failure of the rock. Therefore, the accumulation of rock debris in front of the conventional cutter is obvious. Whereas, the conical cutter is conducive to the cuttings transport, relieving the effect of drilling stickiness slip.
- (3) Carbonate rock with calcite as the main component tends to form blocky rock debris by conical cutter. The cuttings generated by the conical cutter resemble a scallop. The surface of the cuttings generated by the conventional cutter is uneven. The height of the cuttings generated by the conical cutter is 0.5 mm higher than that generated by the conventional cutter. The ability to penetrate the carbonate rock of the conical cutter is stronger.
- (4) At different cutting depths, the conical cutter consistently creates asymmetric jagged brittle tensile fracture zones on both sides of the cutting groove. Conversely, the damage mode of carbonate rock by conventional cutter is mainly plastic deformation at the cutting depth of 1.0 mm. The brittle fracture index of the conical cutter is generally twice that of the conventional cutter, indicating superior utilization of brittle fracture capabilities, particularly for carbonate rock.
- (5) However, due to the particularity of the cutter shape, the interaction area between the conical cutter and the rock is not as large as that of conventional cutter. As a result, under the same cutting conditions, the rock breaking volume of conical cutter is not as good as that of conventional cutter. This is a disadvantage of conical cutter. Therefore, conical

cutter is generally used in conjunction with conventional cutter to break rocks.

Since carbonate rocks are buried in high-temperature environments underground, however, the single cutter cutting tests were carried out under normal temperatures. Therefore, it is suggested to carry out single cutter cutting tests at high temperatures.

CRediT authorship contribution statement

Xin-Kang Fu: Writing — review & editing, Writing — original draft, Methodology, Investigation. **Chao Xiong:** Validation, Supervision, Conceptualization. **Huai-Zhong Shi:** Resources, Project administration. **Wen-Hao He:** Resources, Project administration, Conceptualization. **Lu-Hai Wang:** Investigation. **Zhong-Wei Huang:** Resources, Project administration, Funding acquisition, Conceptualization.

Declaration of interest statement

The authors declare that they have no known competing financial interests or personal relationships that could have appeared to influence the work reported in this paper.

Acknowledgments

This work was supported by the NSFC Key International (Regional) Cooperative Research Projects (No. 52020105001), National Natural Science Foundation of China (52304014), China Postdoctoral Science Foundation funded project (2023M733873), the Science Foundation of China University of Petroleum, Beijing (No. 2462023SZBH003) and General Program of National Natural Science Foundation of China (52374016, 52274016).

References

Al-Shargabi, M., Davoodi, S., Wood, D.A., Ali, Mohsen, Rukavishnikov, Valeriy, Minaev, S., Konstantin, M., 2023. A critical review of self-diverting acid treatments applied to carbonate oil and gas reservoirs. Petrol. Sci. 20 (2), 922–950. https://doi.org/10.1016/j.petsci.2022.10.005.

Cheng, Z., Sheng, M., Li, G.S., Huang, Z.W., Shi, H.Z., Dai, X.W., Guo, Z.Q., 2019. Cracks imaging in linear cutting tests with a PDC cutter: characteristics and development sequence of cracks in the rock. J. Petrol. Sci. Eng. 179, 1151–1158. https:// doi.org/10.1016/j.petrol.2019.04.053.

Dai, X.W., Huang, Z.W., Shi, H.Z., Cheng, Z., Xiong, C., Wu, X.G., Zhang, H.Y., 2020. Rock failure analysis based on the cutting force in the single PDC cutter tests. J. Petrol. Sci. Eng. 194, 107339. https://doi.org/10.1016/j.petrol.2020.107339.

Dai, X.W., Huang, Z.W., Shi, H.Z., Wu, X.G., Xiong, C., 2021a. Cutting force as an index to identify the ductile-brittle failure modes in rock cutting. Int. J. Rock. Mech. Min. 146, 104834. https://doi.org/10.1016/ji.ijrmms.2021.104834.

Dai, X.W., Huang, Z.W., Zou, W.C., Wu, X.G., Shi, H.Z., 2021b. Failure characteristics of rocks subjected to PDC cutter indentation. J. Petrol. Sci. Eng. 207, 108992. https://doi.org/10.1016/j.petrol.2021.108992.

- Fu, X.K., Huang, Z.W., Shi, H.Z., Wu, X.G., He, S.L., Xiong, C., He, W.H., 2023. Comparative analysis on characteristics of cutting carbonate rocks with conical and planar cutters. Chin Petrol. Mach. 51 (7), 59–67. https://doi.org/10.16082/ j.cnki.issn.1001-4578.2023.07.008 (in Chinese).
- He, X.Q., Xu, C.S., Peng, K., Huang, G., 2017. On the critical failure mode transition depth for rock cutting with different back rake angles. Tunn. Undergr. Space Technol. 63, 95–105. https://doi.org/10.1016/j.tust.2016.12.012.
- Jamali, S., Wittig, V., Börner, J., Bracke, R., Ostendorf, A., 2019. Application of high powered Laser Technology to alter hard rock properties towards lower strength materials for more efficient drilling, mining, and Geothermal Energy production. Geomech. Energy. Envir. 20, 100112. https://doi.org/10.1016/ i.gete.2019.01.001.
- Jin, Z.J., Cai, X.Y., Liu, J.L., Zhang, Y., Cheng, Z., 2018. The recent exploration progress and resource development strategy of China Petroleum and Chemical Corporation. Chin. Petrol. Explor. 23 (1), 14–25. https://doi.org/10.3969/j.issn.1672-7703 2018 01 002 (in Chinese)
- Liu, W., Li, Y., Gao, D.L., 2024. New understandings of the applications of PDC cutters in oil and gas drilling. Int. J. Refract. Met. H. 122, 106724. https://doi.org/10.1016/i.iirmhm.2024.106724.
- Liu, W.J., Zhu, X.H., Jing, J., 2018. The analysis of ductile-brittle failure mode transition in rock cutting. J. Petrol. Sci. Eng. 163, 311–319. https://doi.org/10.1016/j.petrol.2017.12.067.
- Ma, Y.S., He, D.F., Cai, X.Y., Liu, B., 2017. Distribution and fundamental science questions for petroleum geology of marine carbonate in China. Acta. Petrol. Sin. 33 (4), 1007–1020 (in Chinese).
- Pittino, G., Galler, R., Antretter, T., Mikl-Resch, M.J., Tichy, R., Ecker, R., Gimpel, M., Kargl, H., 2015. Numerical analysis of the rock cutting process based on a twoparameter description of tensile strength using the weibull theory. In: Proceedings of 13th ISRM International Congress of Rock Mechanics. ISRM-13CONGRESS-, pp. 2015–2306.
- Pryhorovska, T.O., Chaplinskiy, S.S., Kudriavtsev, I.O., 2015. Finite element modelling of rock mass cutting by cutters for PDC drill bits. Petrol. Explor. Dev. 42 (6), 812–816. https://doi.org/10.11698/PED.2015.06.16 (in Chinese).
- Radhakrishnan, V., Chuttani, A., Anggrani, F., Nan, H., Onkvisit, P.S., 2016. Conical diamond element technology delivers step change in directional drilling performance. In: Proceedings of IADC/SPE Asia Pacific Drilling Technology Conference. D021S009R010.
- Raymond, D.W., Knudsen, S.D., Blankenship, D.A., Bjomstad, S., Barbour, J., Drilling, B., Schen, A., Downhole, N.O.V., 2012. PDC bits outperform

- conventional bit in geothermal drilling project. In: Proceedings of Research Org. Sponsor Org.: USDOE National Nuclear Security Administration (NNSA), Albuquerque, NM (United States). Sandia National Lab. (SNL-NM).
- Rostamsowlat, I., Evans, B., Kwon, H.J., 2022. A review of the frictional contact in rock cutting with a PDC bit. J. Petrol. Sci. Eng. 208, 109665. https://doi.org/ 10.1016/j.petrol.2021.109665.
- Sun, Y.X., Zou, D.Y., Hou, X.T., Dou, N.H., 2014. Test of force of conical PDC cutter during rock plow-breaking. Chin. Petrol. Mach. 42, 23–26 (in Chinese).
- Sun, Y.X., Zou, D.Y., Xu, C.K., Guo, Y.L., 2015. Contrast experiment on conical PDC cutter and conventional PDC cutter. Sci. Technol. Eng. 15 (36), 159–162. https://doi.org/10.3969/i.issn.1671-1815.2015.36.027 (in Chinese).
- Xiong, C., Dai, X.W., Shi, H.Z., Huang, Z.W., Chen, Z.L., Zhao, H.Q., 2020a. Investigation on rock breakage mechanism of stinger PDC cutter and hybrid cutter arrangement design. In: Proceedings of 54th U.S. Rock Mechanics/Geomechanics Symposium. ARMA-2020-1419.
- Xiong, C., Huang, Z.W., Shi, H.Z., Yang, R.Y., Wu, G., Chen, H., He, W.H., 2023a. Performances of a Stinger PDC cutter breaking granite: cutting force and mechanical specific energy in single cutter tests. Petrol. Sci. 20 (2), 1087–1103. https://doi.org/10.1016/j.petsci.2022.10.006.
- Xiong, C., Huang, Z.W., Shi, H.Z., Chen, H., Chen, Z.L., He, W.H., Zhang, B., 2023b. Investigations on the Stinger PDC cutter breaking granitoid under in-situ stress and hydrostatic pressure conditions. Int. J. Rock. Mech. Min. 164, 105312. https://doi.org/10.1016/j.iirmms.2022.105312.
- Xiong, C., Huang, Z.W., Shi, H.Z., Zhang, B., Chalaturnyk, R., 2022. Experimental investigation into mixed tool cutting of granite with stinger PDC cutters and conventional PDC cutters. Rock Mech. Rock Eng. 55 (2), 813–835. https:// doi.org/10.1007/s00603-021-02680-z.
- Xiong, C., Huang, Z.W., Yang, R.Y., Sheng, M., Shi, H.Z., Dai, X.W., Wu, X.G., Zhang, S.K., 2020b. Comparative analysis cutting characteristics of stinger PDC cutter and conventional PDC cutter. J. Petrol. Sci. Eng. 189, 106792. https://doi.org/10.1016/j.petrol.2019.106792.
- Zeng, Y.J., Jin, Y., Zhou, Y.C., Chen, J.H., Li, M., Guang, X.J., Lu, Y.H., 2023. Progress and prospect of deep oil & gas drilling and production technologies. Rev. Comment. 2 (2), 32–46. https://doi.org/10.3981/j.issn.2097-0781.2023.02.003 (in Chinese).
- Zhao, W.Z., Hu, S.Y., Liu, W., Wang, T.S., Li, Y.X., 2014. Petroleum geological features and exploration prospect of deep marine carbonate rocks in China onshore: a further discussion. Nat. Gas. Ind. B. 1 (1), 14–23. https://doi.org/10.1016/ i.ngib.2014.10.002.
- Zhou, Y.N., Lin, J.S., 2014. Modeling the ductile—brittle failure mode transition in rock cutting. Eng. Fract. Mech. 127, 135–147. https://doi.org/10.1016/ j.engfracmech.2014.05.020.